The Effect of Aerodynamic Evaluators on the Multi-Objective Optimization of Flatback Airfoils

M Miller[1], K Lee Slew[1] and E Matida[2]

[1]Graduate Student, Mechanical and Aerospace Engineering, Carleton University, 1125 Colonel By Drive, K1S 5B6, Ottawa, Canada
[2]Associate Professor, Mechanical and Aerospace Engineering, Carleton University, 1125 Colonel By Drive, K1S 5B6, Ottawa, Canada

E-mail: MikeMiller@cmail.carleton.ca

Abstract. With the long lengths of today's wind turbine rotor blades, there is a need to reduce the mass, thereby requiring stiffer airfoils, while maintaining the aerodynamic efficiency of the airfoils, particularly in the inboard region of the blade where structural demands are highest. Using a genetic algorithm, the multi-objective aero-structural optimization of 30% thick flatback airfoils was systematically performed for a variety of aerodynamic evaluators such as lift-to-drag ratio (C_L/C_D), torque (C_T), and torque-to-thrust ratio (C_T/C_N) to determine their influence on airfoil shape and performance. The airfoil optimized for C_T possessed a 4.8% thick trailing-edge, and a rather blunt leading-edge region which creates high levels of lift and correspondingly, drag. It's ability to maintain similar levels of lift and drag under forced transition conditions proved it's insensitivity to roughness. The airfoil optimized for C_L/C_D displayed relatively poor insensitivity to roughness due to the rather aft-located free transition points. The C_T/C_N optimized airfoil was found to have a very similar shape to that of the C_L/C_D airfoil, with a slightly more blunt leading-edge which aided in providing higher levels of lift and moderate insensitivity to roughness. The influence of the chosen aerodynamic evaluator under the specified conditions and constraints in the optimization of wind turbine airfoils is shown to have a direct impact on the airfoil shape and performance.

1. Introduction

With the ever-increasing demand for green energy, wind turbine blades are becoming longer in an attempt to capture more energy from the wind. According to the square-cube law [1], the energy capture of a wind turbine rotor increases with the square of it's diameter, whereas rotor mass increases with the cube of it's diameter. Although longer rotor blades allow for more energy capture, significantly higher loading is experienced due to the increase in blade mass, as well as aerodynamic forces acting on the blade. As the first link between the conversion of the wind's kinetic energy to rotational torque, proper airfoil design and selection are vital aspects in the creation of a highly efficient wind turbine. With ever-increasing blade lengths, the optimization of airfoils which are both aerodynamically effective, and structurally suitable, must be employed.

The optimization of airfoils for the inner region of the blade require the use of thick airfoils, oftentimes utilizing the characteristic flatback profile, which offer high lift characteristics, good insensitivity to roughness, as well as high sectional moment of inertia thereby granting the design of an efficient, lightweight and low cost rotor blade. Wind turbine airfoils are typically optimized

for coefficient of lift-to-drag ratio (C_L/C_D) [2–5], or possibly coefficient of torque (C_T) [6], however, no study to the author's knowledge has been systematically performed to determine the effect of the aerodynamic evaluator on the airfoil design. Although the Riso-B1 airfoils optimized for C_T were found to possess favorable leading-edge roughness insensitivity [6], the later generation Riso-C2 airfoils [7], which were optimized for C_L/C_D, outperformed the Riso-B1 airfoils for many parameters, including roughness insensitivity, indicating the importance of design constraints and objectives.

In this study, the multi-objective optimization of 30% thick flatback airfoils will be analyzed when considering various aerodynamic evaluators such as C_L/C_D, C_T and C_T/C_N. A specified set of constraints and objectives will be utilized for all cases such that this is a consistent variable throughout. Structural characteristics such as location of maximum thickness, sectional moment of inertia, and trailing-edge thickness will be taken into consideration. The outcome of this study is to provide better insight into airfoil design decisions and their respective effects on airfoil shape and performance through the systematic variance of aerodynamic evaluators.

2. Methods

The multi-objective, aero-structural optimization of the flatback airfoils was performed using a genetic algorithm coupled with XFOIL to determine the aerodynamic performance of the airfoil, while the structural performance was evaluated based on the airfoil's sectional moment of inertia (I_{XX})– a function of its shape. The I_{XX} is a measure of an object's resistance to bending about an axis, in this case the neutral axis of the airfoil which is parallel to the chord.

XFOIL employs a viscid/inviscid panel method to solve the flow around airfoils [8] and although it has been found to over-predict lift and under-predict drag in several other studies [9–12], particularly under post-stall conditions, it's quick computational time makes it ideally suited for optimization schemes where thousands of computations must be performed in a reasonable time. An amplification factor (N) of 9 was used for the e^N method employed in XFOIL for predicting transition. It is suggested that XFOIL's predicted airfoil performance is experimentally validated once a design is finalized, especially when large overall thickness and trailing-edge thicknesses are present.

Using two separate Bezier curves defining the top and bottom airfoil surfaces, with a total of 13 Bezier control points, the shape of the airfoil was generated. As seen in Figure 1, each of the control points were permitted to move in two directions, with the exception of the control points at the leading and trailing-edge, which were only permitted to move in the vertical direction. The points near the leading-edge must move collinearly such that the joint between the top and bottom surface Bezier curves is smooth at the leading-edge. The bounds of the control points were initially set such that a large portion of the design space could be explored, however were reduced in size following the analysis of several optimizations. This resulted in a more focused optimization which aided in achieving faster convergence times. Constraints on the movement of the control points were selected such that only reasonable airfoil shapes were obtained. The control points defining the trailing-edge were constrained to move symmetrically about the chord to eliminate the need to de-rotate the airfoil. Trailing-edge thicknesses of 1%-20% were permitted, and for comparison purposes between airfoils, the maximum relative thickness was constrained to be 30%.

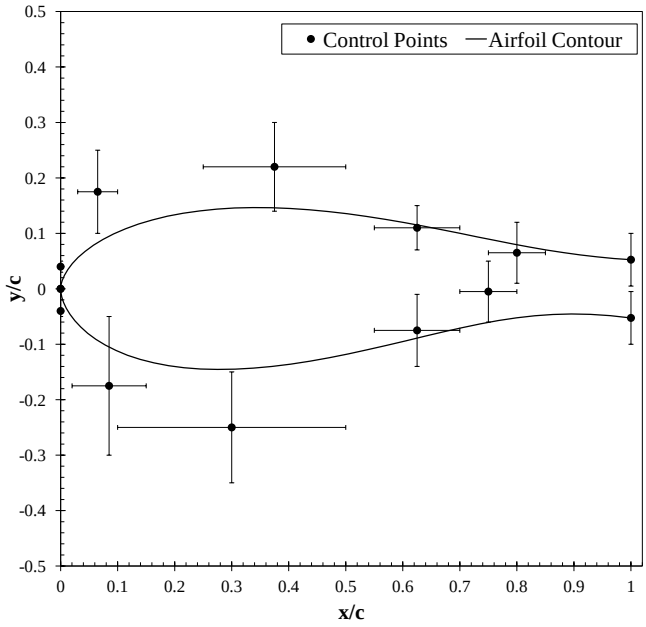

Figure 1. The 13 Bezier control points, along with their respective bounds, which create the airfoil contour

The airfoils were optimized at $Re = 6\times10^6$ and $Ma = 0.1$ which are typical values for inboard sections of multi-MegaWatt wind turbines [13, 14]. The evaluation of aerodynamic performance was varied between C_L/C_D, C_T, and C_T/C_N at angles of attack (AOA) defined as $\alpha = 7^\circ \pm 3^\circ$ to account for wind gusts and off-design conditions. Since this study is solely focused on the optimization of the airfoil itself, and not the overall blade design, the influential effects of camber on the airfoil optimization results were eliminated by formulating all aerodynamic evaluators relative to the zero-lift AOA ($\alpha_{C_{L0}}$) as shown in Equation 1 [6]. Note that all results in this study are presented according to Equation 1.

$$\alpha = \alpha_{original} - \alpha_{C_{L0}} \tag{1}$$

C_T and C_N were evaluated based on Equations 2 and 3, where β is the geometric twist. This formulation, as illustrated in Figure 2, shows that as the flow angle ($\beta + \alpha$) increases, the contribution to torque due to the lift forces becomes increasingly significant. Thus, at inboard sections of the blade where flow angles are large, lift is of particular importance, whereas at outboard sections of the blade where flow angles are small, lift contributes primarily to rotor thrust, therefore an appropriate balance of lift and drag is of particular importance. In this work, the geometric twist of the airfoil section is assumed to be zero, i.e. $\beta = 0$. In a full rotor blade design, the blade geometric twist would be adjusted such that the design angle of attack is met.

$$C_T = C_L \sin(\beta + \alpha) - C_D \cos(\beta + \alpha) \tag{2}$$

$$C_N = C_L \cos(\beta + \alpha) + C_D \sin(\beta + \alpha) \tag{3}$$

As stated in the work performed by Fuglsang *et al.* [6], when optimizing for C_L/C_D, forced transition at angles of attack below C_{Lmax} will inevitably increase C_D. A slight increase in C_D will result in a significant decrease in C_L/C_D, therefore the optimization algorithm will likely favor airfoils with low C_D that comes as a result of largely laminar flow. It is hypothesized by the present authors that airfoils optimized for C_T and C_T/C_N, as defined by Equations 2

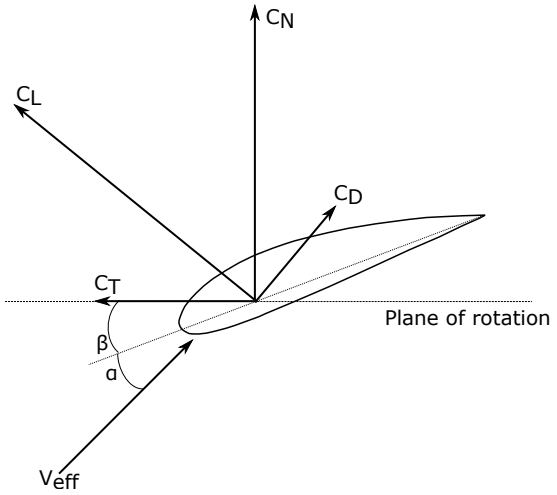

Figure 2. Aerodynamic force coefficients acting on a wind turbine airfoil cross-section

and 3, will be less affected by higher values of C_D and therefore will possess larger trailing-edge thicknesses which aids in the insensitivity to roughness, overall maximum C_L (C_{Lmax}), as well as structural characteristics.

Although inboard sections of rotor blades are typically less affected by contamination and erosion than outboard sections, as rotor blades continue to increase in size, thicker airfoils will become more prominent at larger radii. For this reason, a 25% and 75% weighted sum of clean and tripped conditions respectively in the α range was implemented to simulate a situation where the majority of the turbine's life is spent in fouled conditions [15]. For tripped conditions, transition was forced in XFOIL at 2% chord and 10% chord on the suction and pressure surfaces respectively to mimic a high degree of leading-edge roughness caused by erosion, contamination and manufacturing imperfections [16, 17]. Insensitivity to leading-edge roughness was ensured by constraining the decrease in C_{Lmax} between clean and tripped conditions to 15%, thereby forcing the suction surface transition to a point near the leading-edge at AOAs close to C_{Lmax}. The aerodynamic performance of each airfoil was integrated over the α range.

Determined through convergence analyses, optimization runs were performed with an appropriate number of generations and population size. Each optimization was repeated to verify that consistent findings were achieved. Since the aerodynamic characteristics of each airfoil were primarily studied in this work, the aerodynamically best performing airfoil from each pareto front of solutions was used for all comparisons.

3. Results and Discussion

3.1. Comparison of Airfoil Shape and Performance

Three airfoils with a maximum thickness of 30%, optimized for C_L/C_D, C_T, and C_T/C_N were generated. As can be seen in Figure 3, the airfoil shapes for the C_L/C_D optimized and C_T/C_N optimized airfoils are quite similar, whereas the C_T optimized airfoil has a different pressure surface shape and the shallowest suction surface. The C_T optimized airfoil's maximum thickness is located at the 28% chord location, and features a 4.8% thick flatback trailing-edge compared to the maximum thickness at the 33% chord location and the 3.9% trailing-edge thickness of the C_L/C_D and C_T/C_N optimized airfoils. Despite these differences, all three airfoils can be considered to be structurally equivalent since they possessed comparable values of I_{XX}.

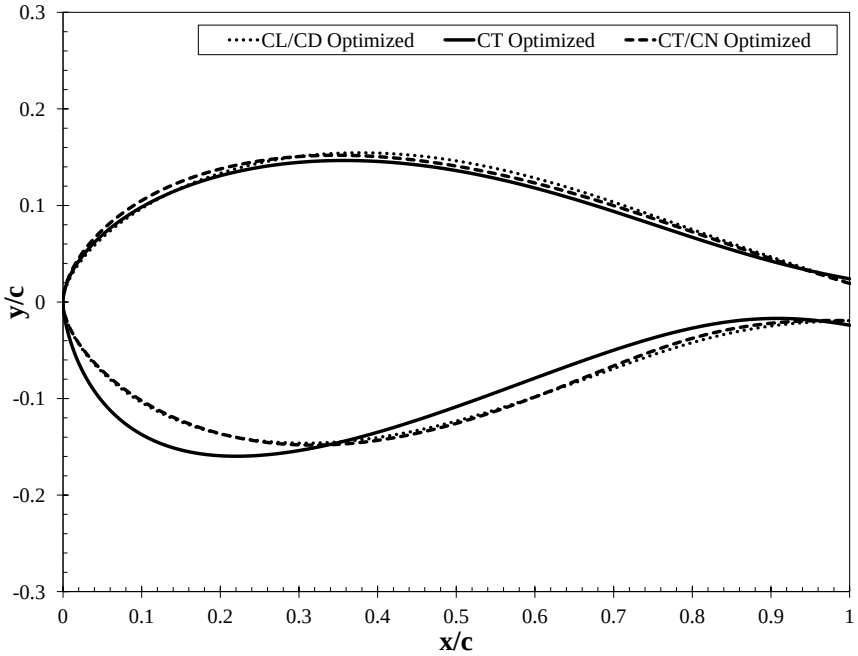

Figure 3. Three 30% thick airfoils optimized for maximum C_L/C_D, C_T, and C_T/C_N

Figures 4 and 5 show the C_L performance of all three airfoils under free and forced transition. In both cases, the C_T optimized airfoil exhibits the largest C_L values thanks to it's slightly larger trailing-edge thickness, which forces pressure recovery to occur in the wake, as well as it's larger camber value of 2.2% compared to the 1.8% of the remaining two airfoils. Under forced transition conditions, the drop in C_L, and inevitable increase in C_D for the C_T optimized airfoil is the least significant of all airfoils. The large trailing-edge, as well as the shallow suction surface results in good insensitivity to roughness. As shown in Figures 6 and 7, large values of C_D come as a by product of not only the thicker trailing-edge, but also due to the more forward-located free transition points on both the suction and pressure surfaces compared to the C_L/C_D and C_T/C_N optimized airfoils. As shown in Figure 8 and 9, the high drag of the C_T optimized airfoil results in a large loss in C_L/C_D performance, whereas the low drag of the C_L/C_D ensures a high aerodynamic efficiency ratio.

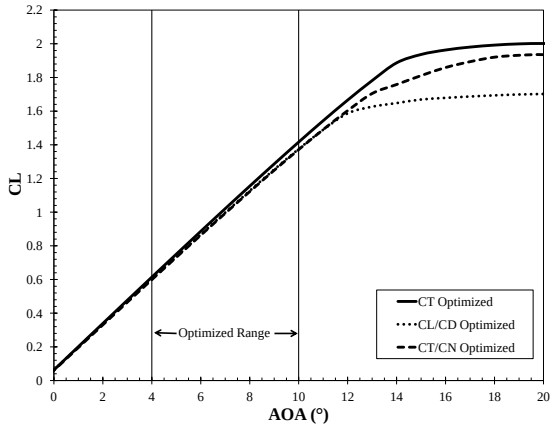

Figure 4. C_L of the airfoils under free transition conditions at $Re = 6 \times 10^6$

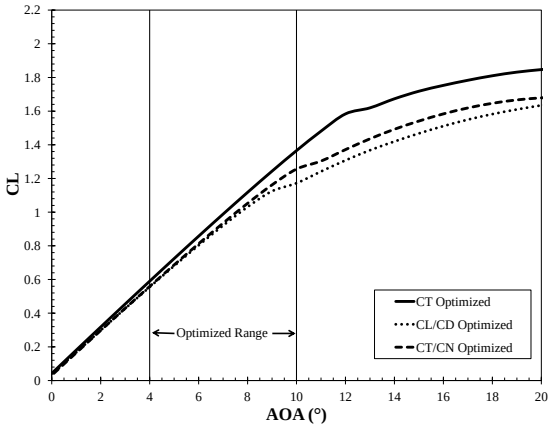

Figure 5. C_L of the airfoils under forced transition conditions at $Re = 6 \times 10^6$

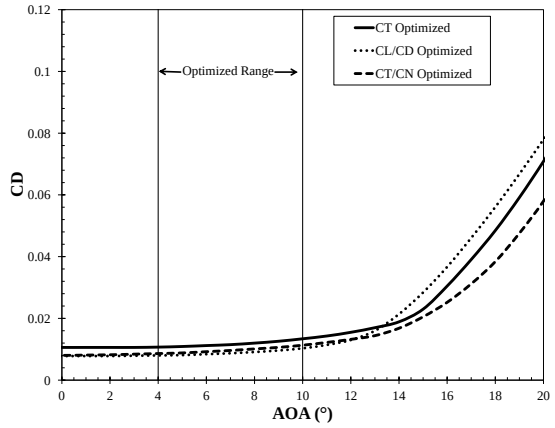

Figure 6. C_D of the airfoils under free transition conditions at $Re = 6 \times 10^6$

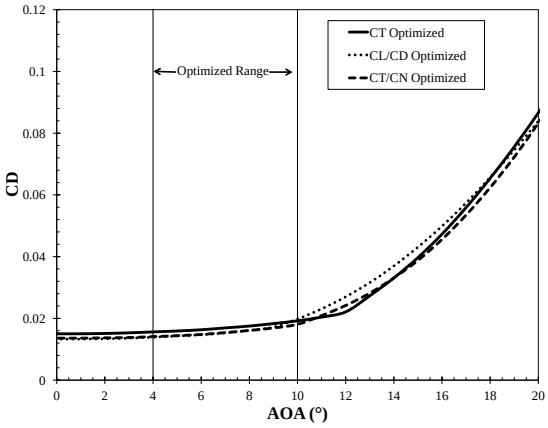

Figure 7. C_D of the airfoils under forced transition conditions at $Re = 6 \times 10^6$

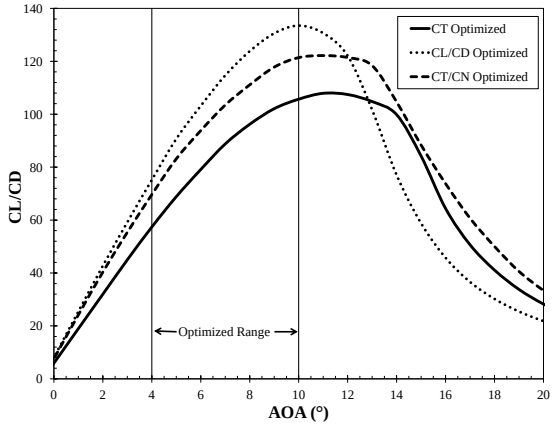

Figure 8. C_L/C_D of the airfoils under free transition conditions at $Re = 6 \times 10^6$

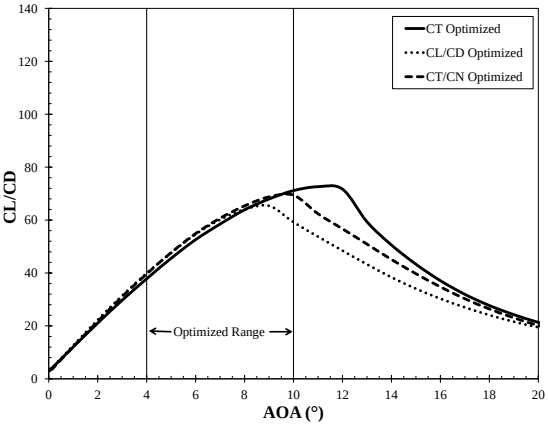

Figure 9. C_L/C_D of the airfoils under forced transition conditions at $Re = 6 \times 10^6$

When comparing the C_L and C_D performance of the C_L/C_D and C_T/C_N optimized airfoils, it can be seen that the C_T/C_N airfoil produces more lift, as well as drag due to the slightly more blunt leading-edge. This blunter leading-edge results in higher coefficients of pressure around the leading-edge region, thereby producing a more adverse pressure gradient, and in turn, a more forward-located transition point on the suction surface compared to the C_L/C_D airfoil. However, under tripped conditions, this already forward-located transition of the C_T/C_N airfoil leads to a less drastic drop in performance. The C_L/C_D optimized airfoil has a large portion of laminar flow over the top and bottom surfaces which helps reduce drag, however, leads to poor relative performance when transition is forced. All three airfoils exhibit rather similar gentle stall characteristics, with no sudden loss of lift in the examined AOA range.

Table 1 highlights some key characteristics of each airfoil, with the number in brackets representing the percent change in value under forced transition conditions. The airfoil optimized for C_T experiences the smallest reduction in lift, and the smallest increase in drag compared to the other two airfoils under tripped conditions. As mentioned earlier, this is due to the already forward-located free transition points which minimizes the diminishing performance effects of the simulated leading-edge roughness. The C_T/C_N optimized airfoil demonstrates leading-edge roughness insensitivity that is in between that of the C_L/C_D and C_T optimized airfoils.

Table 1. Key aerodynamic characteristics for the three airfoils. Numbers in brackets represent the percent change under forced transition

Key Airfoil Characteristics				
Optimized For:	C_L@7°	C_D@7°	Free trans. top @7° (x/c)	Free trans. bottom @7° (x/c)
C_L/C_D	1.00 (-8.0%)	0.0087 (+55.0%)	0.407	0.480
C_T	1.02 (-3.2%)	0.0115 (+38.0%)	0.338	0.330
C_T/C_N	0.99 (-6.1%)	0.0096 (+46.4%)	0.317	0.488

3.2. C_L/C_D Performance

Figure 10 shows the weighted sum performance (25% free, 75% forced transition) of the three airfoils in the α range when C_L/C_D is assigned as the aerodynamic evaluator. Despite differences in roughness insensitivity, the C_L/C_D and C_T/C_N optimized airfoils performed similarly when the integral of the C_L/C_D curve over the α range was taken, with the C_L/C_D slightly outperforming the rest. The C_T optimized airfoil showed the poorest C_L/C_D performance due to its large values of C_D which proved to decrease the lift-to-drag ratio noticeably, however, both the C_T and C_T/C_N airfoils began to show improvement at large AOA due to better insensitivity to roughness caused by the free transition point being closer to the location of forced transition.

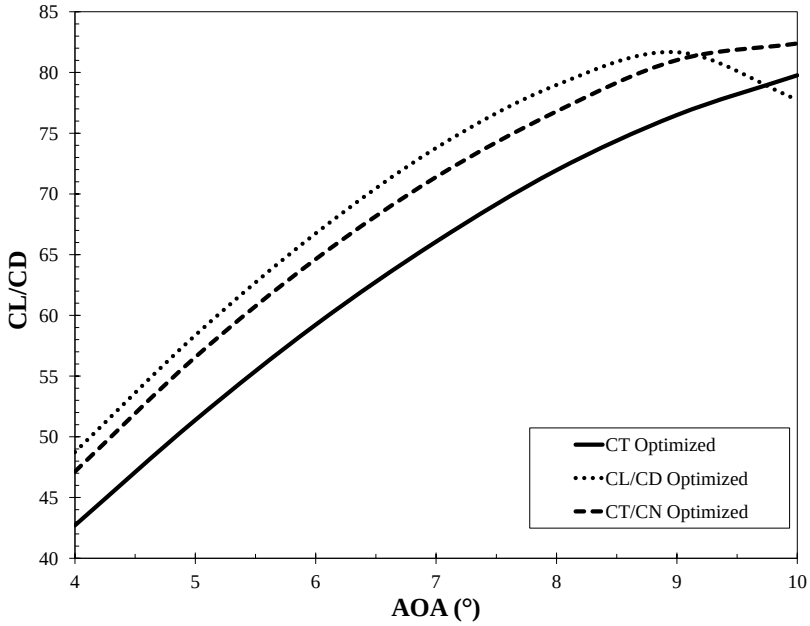

Figure 10. The C_L/C_D weighted sum (25% free, 75% forced transition) performance of each of the three airfoils in the α range

3.3. C_T Performance

As shown in Figure 11, when C_T was assigned as the aerodynamic evaluator in the optimization scheme, the weighted sum performance of the C_T optimized airfoil surpassed the remaining two airfoils over the entire α range. It's ability to retain similar levels of lift and drag under free and forced conditions demonstrated it's insensitivity to roughness. In turn, the high levels of lift that were maintained proved to be dominant over the relatively high levels of C_D in the calculation of C_T. Under forced transition, the C_T/C_N optimized airfoil was able to maintain reasonably high levels of lift, without too large of an increase in drag which resulted in it outperforming the C_L/C_D optimized airfoil which exhibits poor insensitivity to roughness.

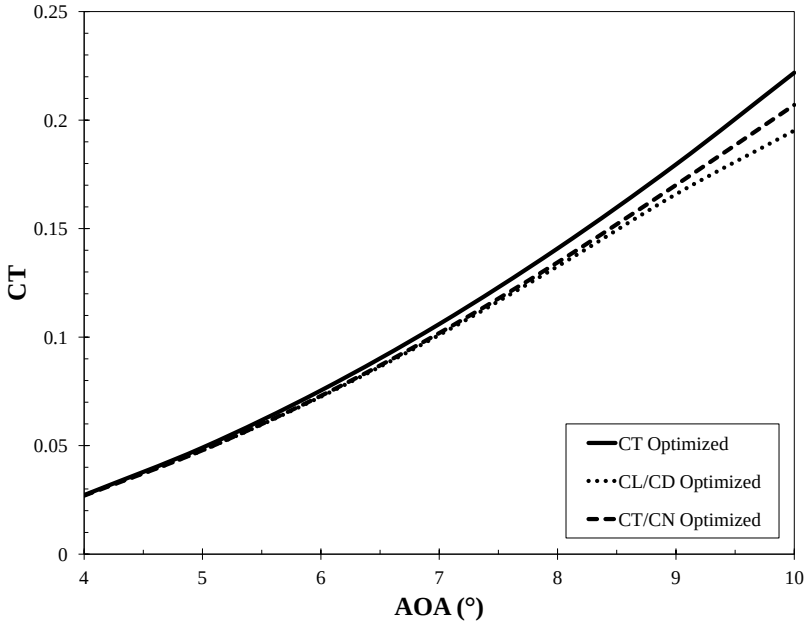

Figure 11. The C_T weighted sum (25% free, 75% forced transition) performance of each of the three airfoils in the α range

3.4. C_T/C_N Performance

From Figure 12, it can be shown that all three airfoils have similar C_T/C_N weighted sum performance over the α range. Closer inspection reveals that for the majority of the α range, the C_T/C_N optimized airfoil is the best performing. In contrast to the plot of C_L/C_D (Figure 10), both the C_T and C_T/C_N plots (Figures 11 and 12 respectively) do not exhibit a discernible drop in performance in the α range– in fact their performance continually increases for increasing AOA. This indicates that the flow angle, in this case the AOA (since $\beta = 0$), has a greater effect on the performance than an inevitable increase in drag caused by forced transition. Therefore, optimizing under the given specified constraints and conditions for C_T or C_T/C_N will produce different airfoil shapes, and in turn performance, than C_L/C_D optimized airfoils.

3.5. Summary

In summary, under the design constraints and objectives, the C_T optimized airfoil favors superior roughness insensitivity at the expense of increased drag values at low AOA. It's high lift performance provides high levels of torque, which is particularly important in the inboard regions of the blade where moment arms are rather short, and allows for a reduction in chord length thereby resulting in a more slender blade design. The C_L/C_D airfoil favors low levels of drag, which aids in producing high lift-to-drag ratios, at the expense of poor roughness insensitivity. The C_T/C_N optimized airfoil offers a balance of low drag and roughness insensitivity, and ensures that the maximum torque-to-thrust ratio is achieved such that acceptable loading characteristics are maintained. All three of the airfoils outperformed the others for their respective aerodynamic evaluator over the α range proving the effectiveness of the optimization routine.

The results in this study are dependent on the specified design constraints and conditions, however, show that differences in airfoil shape and performance are apparent depending on the aerodynamic evaluator chosen by the designer. If less consideration for contaminated conditions was introduced by using a more balanced weighted-sum of clean and tripped conditions, it is suspected that all three airfoils will begin to converge in shape. A low weighting factor towards simulated roughness will likely lead to airfoils that are more similar in shape and performance to the C_L/C_D optimized airfoil obtained in this study which generally displayed the best performance under clean conditions.

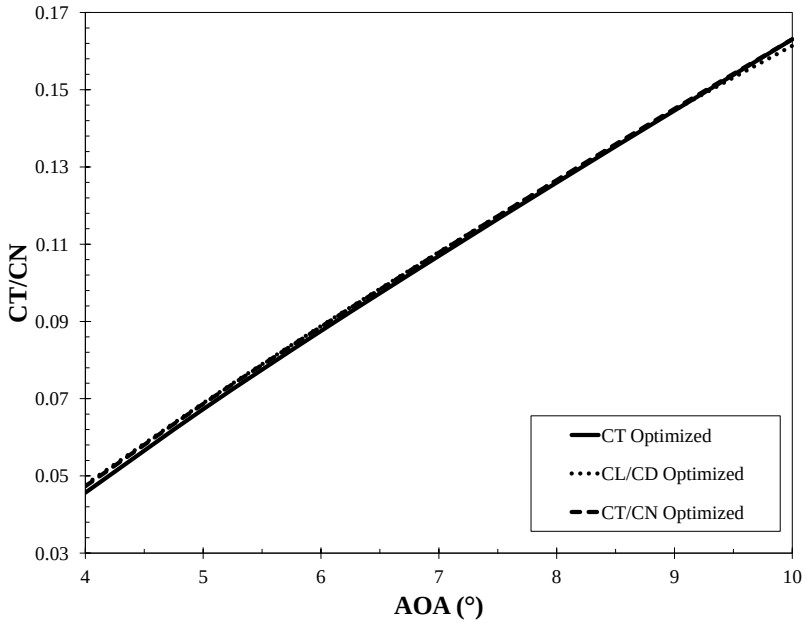

Figure 12. The C_T/C_N weighted sum (25% free, 75% forced transition) performance of each of the three airfoils in the α range

4. Future Work

Further analysis of the effect of varying aerodynamic evaluators for different AOA ranges, ratios of clean and tripped weighted sums, forced transition locations, and roughness insensitivity criteria may be explored utilizing the optimization tool developed in this work. Additionally, the effects of airfoil aeroacoustics may be added as an optimization objective. Furthermore, the effects of rotation, as well as the improved prediction of C_{Lmax}, can be incorporated into the design optimization by using RFOIL [18]. A hybrid optimization scheme consisting of a genetic algorithm which employs a computationally fast tool such as XFOIL or RFOIL used to explore a large design space, followed by a gradient based technique which uses a higher fidelity tool such as CFD to refine the results may allow for more optimal results. Additionally, a more accurate structural evaluator can be incorporated into the design optimization and coupled to a BEM technique to perform the aero-structural optimization of the airfoils and blade in tandem. Lastly, wind tunnel experiments must be performed on the airfoils to verify the results obtained using XFOIL.

5. Conclusion

Multi-objective, aero-structural optimization of airfoils with 30% thickness was performed to determine the effects of aerodynamic evaluators such as C_L/C_D, C_T, and C_T/C_N on airfoil performance and shape. Under invariable objectives and constraints, similar results were obtained for airfoils optimized for C_L/C_D and C_T/C_N, however, the airfoil optimized for C_T possessed a slightly thicker trailing-edge and a more blunt leading-edge providing it with higher levels of lift and better roughness insensitivity. The C_T/C_N optimized airfoil possessed insensitivity to roughness that was in between that of the C_T airfoil and the C_L/C_D airfoil. Airfoils optimized for C_L/C_D under the specified objectives and constraints performed relatively poorly under forced transition due to the inherent increase in drag.

Given the set of design constraints and conditions used in this optimization study, noticeable differences were attained for both airfoil shape and performance depending on the aerodynamic evaluator used. The constraints and objectives of the optimization will surely have an effect on the outcome of the design, and depending on the aerodynamic evaluator used, should be altered

to meet the design goals. If a different weighted-sum consideration, or criteria for roughness insensitivity is used, it is likely that the airfoils will possess a different shape and performance. Thus, the influence of the aerodynamic evaluator was found to have a notable effect on the design of 30% thick wind turbine airfoils for the described constraints and objectives in this work.

References

[1] Spera D 2009 *Wind Turbine Technology- Fundamental Concepts of Wind Turbine Engineering* (New York, NY: ASME)
[2] Winnemoller T and Van Dam C 2007 *Journal of Aircraft* **44** 232–240
[3] Chen X and Agarwal R 2012 *Journal of Aircraft* **49** 622–629
[4] Cooperman A, McLennan A, Chow R, Baker J and van Dam, CP 2010 Aerodynamic Performance of Thick Blunt Trailing Edge Airfoils *28th AIAA Applied Aerodynamics Conference* (Chicago, IL: American Institute of Aeronautics and Astronautics)
[5] Grasso F 2012 Hybrid Optimization for Wind Turbine Thick Airfoils *53rd AIAA/ASME/ASCE/AHS/ASC Structures, Structural Dynamics and Materials Conference* (Honolulu, HI: American Institute of Aeronautics and Astronautics)
[6] Fuglsang P, Bak C, Gaunaa M and Antoniou I 2004 *Journal of Solar Energy Engineering* **126** 1002–1010
[7] Bak C, Andersen P, Madsen H, Gaunaa M, Fuglsang P and Bove S 2008 Design and Verification of Airfoils Resistant to Surface Contamination and Turbulence Intensity *26th AIAA Applied Aerodynamics Conference* (Honolulu, HI: American Institute of Aeronautics and Astronautics)
[8] Drela M 1989 XFOIL: An Analysis and Design System for Low Reynolds Number Airfoils *Low Reynolds Number Aerodynamics* vol 54 ed Mueller T J (Notre Dame, IN) pp 1–12
[9] Bertagnolio F, Sorensen N, Johansen J and Fuglsang P 2001 Wind Turbine Airfoil Catalogue Tech. rep. Riso National Laboratory Roskilde, DK
[10] Timmer W and van Rooy R 1992 *Journal of Wind Engineering and Industrial Aerodynamics* **39** 151–160
[11] Maughmer M and Coder J 2010 Comparisons of Theoretical Methods for Predicting Airfoil Aerodynamic Characteristics Tech. rep. U.S. Army Research, Development and Engineering Command Port Matilda, PA
[12] Shen W, Zhu W, Fischer A, Garcia N, Cheng J, Chen J and Madsen J 2012 Validation of the CQU-DTU-LN1 series of airfoils *The Science of Making Torque from Wind* (Oldenburg, DE)
[13] Ge M, Tian D and Deng Y 2014 Reynolds Number Effect on the Optimization of a Wind Turbine Blade for Maximum Aerodynamic Efficiency *Journal of Energy Engineering*
[14] Fuglsang P, Antoniou I, Dahl K and Madsen H 1998 Wind Tunnel Tests of the FFA-W-241, FFA-W3-301 and NACA63-430 Airfoils Tech. rep. Riso National Laboratory Roskilde, DK
[15] Gutierrez C 2014 *Aerodynamic and Aeroelastic Design of Low Wind Speed Wind Turbine Blades* Master's thesis Technical University of Denmark Lyngby, DK
[16] Ehrmann R, White E, Maniaci C, Chow R, Langel C and van Dam C 2013 Realistic Leading-Edge Roughness Effects on Airfoil Performance *31st AIAA Applied Aerodynamics Conference* (AIAA)
[17] Sareen A, Sapre C and Selig M 2014 Effects of Leading Edge Erosion on Wind Turbine Blade Performance *Wind Energy* 17 pp 1532–1542
[18] van Rooij R 1996 Modification of the Boundary Layer Calculation in RFOIL for Improved Airfoil Stall Prediction Tech. rep. Delft University of Technology